Role of active changes in venous capacity by the carotid baroreflex: Analysis with a mathematical model

Article *in* The American journal of physiology · January 1995

DOI: 10.1152/ajpheart.1994.267.6.H2531 · Source: PubMed

3 authors, including:

Mauro Ursino
University of Bologna
306 PUBLICATIONS **4,909** CITATIONS

SEE PROFILE

Role of active changes in venous capacity by the carotid baroreflex: analysis with a mathematical model

M. URSINO, M. ANTONUCCI, AND E. BELARDINELLI
Department of Electronics, Computer Science and Systems, University of Bologna, 40136 Bologna, Italy

Ursino, M., M. Antonucci, and E. Belardinelli. Role of active changes in venous capacity by the carotid baroreflex: analysis with a mathematical model. *Am. J. Physiol.* 267 (*Heart Circ. Physiol.* 36): H2531–H2546, 1994.—To elucidate the role of venous capacity active changes in short-term cardiovascular homeostasis, a mathematical model of the carotid-sinus baroreflex system has been developed. In the model the cardiovascular system is represented as the series arrangement of six lumped compartments, which synthesize the fundamental hemodynamic properties of the systemic arterial, systemic venous, pulmonary arterial, and pulmonary venous circulations as well as of the left and right cardiac volumes. Cardiac outputs from the left and right ventricles are computed as a function of both downstream arterial pressure (afterload) and upstream atrial pressure (preload). Four distinct feedback regulatory mechanisms, working on systemic arterial resistance, heart rate, systemic venous unstressed volume, and systemic venous compliance, are assumed to operate on the cardiovascular system in response to carotid sinus pressure changes. All model parameters, both in the cardiovascular system and in feedback regulatory mechanisms, have been assigned on the basis of physiological data now available. The model is used here to simulate the pattern of the main hemodynamic quantities in the short time period (1–2 min) after acute carotid sinus activation in vagotomized subjects. Simulation results indicate that the model can reproduce experimental data quite well, with reference both to open-loop experiments and to an acute blood hemorrhage performed in closed-loop conditions. Moreover, computer simulations indicate that active changes in venous unstressed volume are of primary importance in regulating cardiac output and systemic arterial pressure during activation of the carotid sinus baroreflex.

short-term cardiovascular homeostasis; carotid sinus baroreflex; cardiac output; acute blood hemorrhage; capacity control

VENOCONSTRICTION and the consequent active venous capacity changes are now thought to play a significant role in the short-term cardiovascular regulation in response to various acute hemodynamic perturbations. Lowering venous capacity, in fact, increases filling pressure for the heart, thus supporting stroke volume and cardiac output and favoring restoration of more correct arterial pressure levels.

Several experimental results on the importance of venous capacity baroreflex control have been gathered in recent years. According to most authors, a decrease in the dog's carotid sinus pressure from 250 to 50 mmHg may cause a reduction in the unstressed volume of systemic veins as great as 7–13 ml/kg body wt (22, 31, 32), whereas venous compliance appears to be only slightly reduced (13, 31, 32). These changes in unstressed volume may be able to maintain sufficient filling pressure for the heart, even in response to significant blood volume losses.

Understanding the exact role of the active venous capacity control and its importance in short-term cardiovascular homeostasis is, however, a difficult task because, as is well known, the baroreflex mechanism acts on several effectors simultaneously, including not only systemic venous capacity (i.e., compliance and unstressed volume) but also systemic arterial resistance, heart rate, and cardiac contractility. All of these actions superimpose themselves in the intact organism in very complex and often unpredictable ways. In particular, the existence of strong nonlinearities, both in the cardiovascular system and in control mechanisms, precludes application of the superimposition of the effects. This means that the global result of several mechanisms acting together may be sharply different from the sum of the single actions individually taken.

A deeper understanding of short-term cardiovascular regulation by the baroreflex system may be achieved using mathematical models. The latter, in fact, are able to manage nonlinearities, multiple feedback regulations, and their mutual dependence in a powerful and sophisticated way.

Various models of the baroreflex system have been proposed in recent decades (e.g., 1, 14, 15), the complexity and completeness of which strictly depend on the particular phenomenon the model is intended to investigate. Grodins (14) first developed a systematic approach to the cardiovascular system, including Starling's law of the heart and multiple equations. The mean values of his variables were in agreement with results of several physiological experiments. The model by Beneken and De Wit (1) distinguishes among 19 peripheral segments and lays particular emphasis on the mechanical description of the heart. The model by Guyton and co-workers (15) is probably the most complete computer description of the cardiovascular system but is especially focused on the long-term rather than the short-term regulation.

As far as we know, however, a detailed mathematical analysis of the possible role of active venous capacity changes in short-term cardiovascular regulation is still

not available. The great amount of accurate and specific data on this mechanism published in recent years now permits such a mathematical analysis to be performed and permits the role of venous capacity changes to be investigated in accurate quantitative terms.

The aim of the present study is to present a model of short-term cardiovascular regulation by the carotid baroreflex system, in which proper emphasis is placed on the possible role of active venous capacity changes. First, the responses of the main effectors (heart rate and contractility, systemic arterial resistance, systemic venous unstressed volume, and systemic venous compliance) to carotid stimulation are separately investigated in open-loop conditions, and then suitable mathematical models for each mechanism are proposed according to available experimental data. Subsequently, the entire system behavior in response to pressure or volume perturbations is simulated in conditions where the different regulatory actions superimpose themselves in complex and mutually dependent ways.

The present model is intended to reproduce only short-term cardiovascular adjustments (time duration < 1–2 min) in response to acute hemodynamic perturbations. Responses in the middle period (5–10 min) cannot be simulated due to the existence of slower compensation phenomena (such as delayed autoregulation, viscoelastic creep, and fluid shifts across capillaries) not included in the present model.

In the present study, only the action of the carotid baroreflex system is investigated. To this end, we focus attention on experiments in which the vagus is cut and the action of the aortic baroreflex is eliminated.

QUALITATIVE MODEL DESCRIPTION

According to the methods usually adopted in Automatic Control Theory, we shall first describe the dynamics of the controlled system (or plant), that is, the cardiovascular system in the absence of regulatory actions. Subsequently, we shall focus attention on the major feedback mechanisms that can operate on this system in response to carotid sinus stimulation.

The Controlled System

The model of the overall cardiovascular system employed in the present work (see the electric analog of Fig. 1) consists of the interconnection between two cardiac and four vascular compartments. The latter reproduce hemodynamics in the systemic arterial, systemic venous, pulmonary arterial, and pulmonary venous vascular beds.

Each vascular compartment is described through traditional windkessel models (i.e., the arrangement of a hydraulic resistance, which takes energy losses and pressure drop into account, and a capacity, which reproduces the amount of blood volume contained within the compartment at a given pressure). We deemed it necessary to distinguish between venous and arterial compartments in the model. In fact, as pointed out by Guyton et al. (16), an increase in arterial resistance causes a significant increase in arterial pressure, whereas it has just a minor effect on cardiac output. By contrast, a similar increase in venous resistance provokes a dramatic fall on venous return hence also on cardiac output. The presence of venous (pulmonary and systemic) resistances in the model may be used, in future works, to simulate hemodynamic alterations, and the consequent regulatory response, induced by venous occlusion or by a collapse of the central veins.

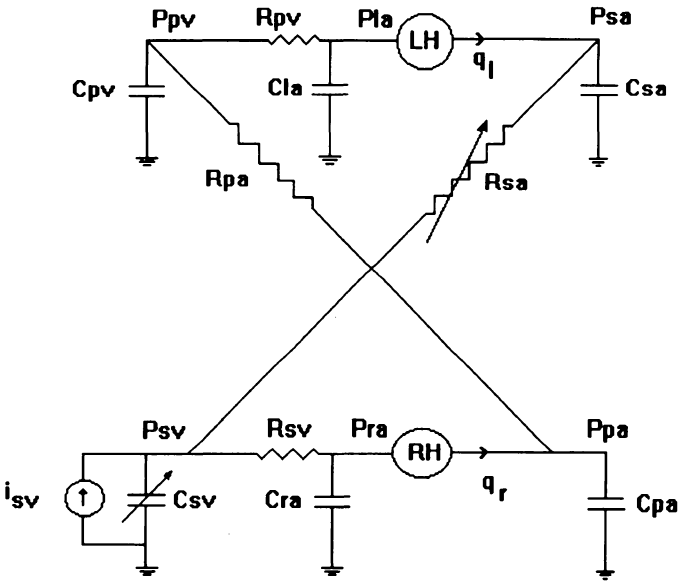

Fig. 1. Electric analog of the cardiovascular system. Hydraulic resistances (R), compliances (C), and pressures (P) were measured in systemic arteries (sa), systemic veins (sv), pulmonary arteries (pa), and pulmonary veins (pv); subscripts la and ra are left (LH) and right (RH) heart, respectively; $\dot{q}_l$ and $\dot{q}_r$ are cardiac output (CO) from left and right ventricles, respectively; and i_{sv}, amount of blood volume injected into (if positive) or subtracted from (if negative) the sv compartment per unit time.

As discussed in *Feedback Regulatory Actions,* the systemic arterial resistance may change as a result of short-term regulatory factors. By contrast, the arterial pulmonary resistance is maintained at a constant value throughout the present work. This choice is acceptable, since, according to data reported by Shoukas (30), the arterial pressure-flow relation can be regarded as linear around a physiological pressure range.

As pointed out by Rothe (25) changes in vascular capacity cannot be adequately described by a single parameter: either the entire pressure-volume characteristic must be specified over the operating range or changes in both compliance and unstressed volume must be separately quantified. In the present work we adopted the same approach used by Shoukas and associates (13, 31, 32) in their classic experiments on the control of venous capacity by the baroreflex system. Like these authors, we assumed that the amount of blood volume in a generic jth compartment depends on the unstressed volume ($V_{u,j}$), defined as the volume-axis intercept of the pressure-volume curve, and the compliance (C_j), which represents the average slope of the pressure-volume curve. Moreover, we also assume that the compliances in Fig. 1 are pressure independent; that is, the pressure-volume curves can be considered as approximately linear over the entire pressure range examined. We can thus write (see also Fig. 2)

$$V_j = V_{u,j} + C_j \cdot P_j = V_{u,j} + V_{e,j} \quad j = \text{sa, sv, pa, pv, ra, la} \quad (1)$$

where V_j and $V_{e,j}$ are total blood volume and excess (or stressed) volume within the jth compartment (the latter quantity represents the amount of blood volume stored by the linear compliances); P_j is transmural pressure in the jth compartment; and subscripts sa, sv, pa, pv, ra, and la are systemic arterial, systemic venous, pulmonary arterial, pulmonary venous, right heart, and left heart, respectively.

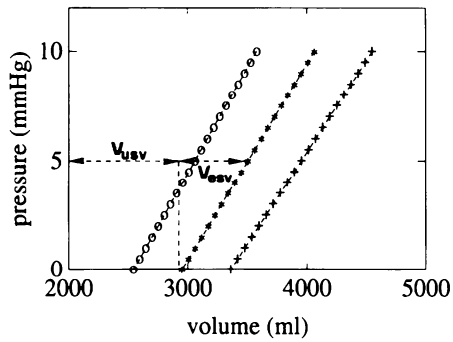

Fig. 2. Model description of systemic venous capacity. P_{sv} is plotted vs. systemic venous blood volume (V_{sv}) at different levels of carotid sinus pressure (P_{cs}). Vascular volume (V) is the sum of 2 terms: unstressed volume ($V_{u,sv}$), defined as the volume-axis intercept of the pressure-volume curve, and excess (or stressed) volume ($V_{e,sv}$), computed as the product of pressure and compliance. Horizontal dotted line at P_{sv} = 5 mmHg is basal level of P_{sv}. *, P_{cs} = 100 mmHg (normal); ○, P_{cs} = 50 mmHg; +, P_{cs} = 150 mmHg. Raising P_{cs} from 50 to 150 mmHg causes a strong increase in $V_{u,sv}$ and a modest increase in compliance. All curves are computed with reference to a 70-kg man.

The use of linear compliances instead of nonlinear pressure-volume characteristics deserves a few comments. We are aware that this is a sharp simplification of the physiological reality because, as is well known, the pressure-volume characteristics of both arteries and veins can exhibit significant nonlinearities. However, this simplification is justified for at least two reasons. First, knowledge of the exact role played by nonlinear terms in pressure-volume characteristics is difficult, since these characteristics not only reflect the behavior of the vascular wall passive elements (for which a monoexponential curve might be adopted) but also are affected by the active reaction of vascular smooth muscle. Contradictory results are reported in the physiological literature on the linearity of pressure-volume relationships over the physiological pressure range (see Ref. 26 for review). Second, most experiments on active control of capacitance vessels are based on the assumption that vascular compliance is pressure independent and that total blood volume can be expressed according to *Eq. 1*. Hence, the use of *Eq. 1* allows direct comparison between experimental data and model simulation curves to be easily achieved.

However, to test the possible role of nonlinear compliances and the errors involved in the use of linear relationships, we also repeated some simulations using exponential pressure-volume curves for the vascular compartments.

Starting from the electric analog of Fig. 1, differential equations describing pressure-flow relationships can be written by imposing mass preservation at the level of the six compliances (see *Eqs. 2–8* in the APPENDIX) and specifying the pattern of cardiac output from the left and right ventricles.

In the model, cardiac volumes are taken into account through linear capacities, involving unstressed volume and compliance, as in *Eq. 1*, while cardiac function is reproduced via two distinct flow generators that simulate the activity of the right and left ventricles, respectively. According to the well-known Frank-Starling mechanism, stroke volume from both ventricles increases with the atrial pressure value. The experimental relationship linking stroke volume to atrial pressure is quite linear in the normal atrial pressure range and exhibits saturation only at rather high pressures (8, 16). Because excessive atrial pressure values were not reached in the present simulations, we considered it sufficient to adopt a linear relationship. Of course, cardiac output is obtained simply in the model as the product of stroke volume and heart frequency.

Furthermore, stroke volume not only depends on atrial pressure (the preload) but also is affected by the afterload against which the heart is working. According to data reported by Downing and Gardner (9), this phenomenon has been taken into account assuming that stroke work slightly increases, while stroke volume decreases, when the afterload rises above normal (see *Eqs. 13* and *14* in the APPENDIX). An example of the dependence of model stroke volume and stroke work on atrial pressure (Frank-Starling mechanism) plotted at different arterial pressure values is shown in Fig. 3 with reference to the left heart. As is clear from Fig. 3 (and in more quantitative terms from *Eqs. 13–14*), a 75-mmHg increase of systemic arterial pressure in our model causes a 32% rise in stroke work from the left ventricle and a 24% reduction in stroke volume. Analogous percentage changes of these quantities during systemic arterial pressure alterations were reported by Downing and Gardner (9).

Feedback Regulatory Actions

The model described above represents the controlled system or plant, that is, the cardiovascular system in the absence of feedback regulatory actions. During carotid sinus activation, however, the carotid baroreflex exerts a strong control action on hematic vessels by modifying smooth muscle tension at the level of systemic arteries and veins and on the heart by changing its pacemaker activity, excitation-contraction coupling, and cardiac strength.

Baroreflex control of hematic vessels produces changes in systemic arterial resistance, systemic venous unstressed volume, and systemic venous compliance. The baroreflex control of the heart, in turn, consists of alterations of heart rate and cardiac contractility.

Whereas the first four regulatory factors can be easily included in our model, the existence of a cardiac contractility control deserves a more critical analysis. As pointed out by several authors (e.g., Ref. 21, p. 262), a satisfactory quantitative index for myocardial contractility does not exist at present. In our model, heart function is described by the slope of

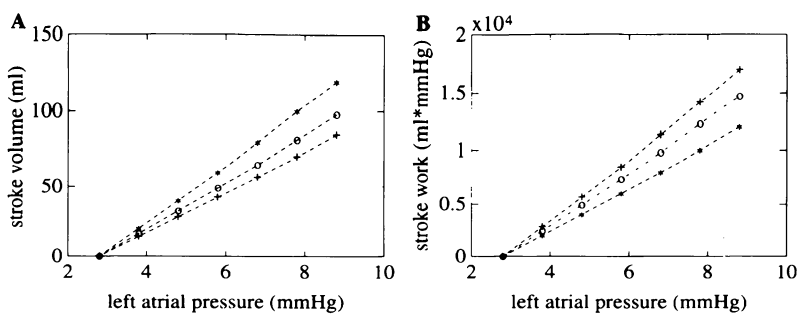

Fig. 3. Model description of cardiac performance at different values of preload and afterload. Stroke volume (*A*) and stroke work (*B*) of left ventricle are plotted against left atrial pressure at different levels of P_{sa}. *, P_{sa} = 100 mmHg (normal); ○, P_{sa} = 150 mmHg; +, P_{sa} = 200 mmHg. Increasing afterload causes a moderate increase in heart work but a decrease in stroke volume, according to Downing and Gardner (9).

the stroke volume-atrial pressure relationship. An increase in heart frequency alone, without a simultaneous increase in contractility, would cause this curve to be shifted down due to a reduction in the duration of diastole. By contrast, an increase in cardiac contractility alone would cause this curve to be shifted up. During carotid sinus stimulation, the effective changes in the stroke volume-atrial pressure relationship may appear contradictory, since they reflect the simultaneous superimposition of these two antagonistic factors (see *Eq. 12*).

Indeed, experimental results derived in conditions of constant afterload indicate that the stroke volume-atrial pressure relationship is either unaffected (8, 9) or mildly affected (18) by carotid sinus activation in the dog. Similarly, Greene and Shoukas (13), in a group of 10 animals, observed inconsistent changes in the stroke volume curve after carotid sinus pressure alterations between 50 and 200 mmHg. According to these data, we decided to maintain the slope of the stroke volume-atrial pressure curve independent of carotid sinus pressure. This choice does not imply the absence of an active control of cardiac force; it simply presumes, lacking more evident quantitative data, that the reinforced cardiac strength induced by baroreflex activation approximately compensate for the shorter time period allowed for cardiac filling.

According to the previous considerations, control actions in the model have been described through the multifeedback block diagram of Fig. 4. As is clear from Fig. 4, four distinct feedback loops have been included. All are elicited by changes in carotid sinus transmural pressure and exert their action on systemic resistance, heart rate, systemic venous unstressed volume, and systemic venous compliance.

The feedback regulatory actions of the first three mechanisms are assumed to work according to the general schema of Fig. 5. This is composed of the series arrangement of two blocks. The first reproduces the nonlinear static response of the baroreflex, which, as is well known, is sigmoid shaped and exhibits a lower threshold and upper saturation (28). The second block, in turn, describes the time dynamic of the baroreceptor response. This has been reproduced using a first-order differential equation, that is, a simple transfer function with a single real pole. The time constant of the transfer function takes the time delay of the regulatory process approximately into account.

We are aware that transfer functions more complex than those employed in the present work have sometimes been proposed in the physiological literature. By way of example, Sagawa (28) indicated a second-order function with a pure latency. Others (1) proposed that the baroreflex response is not only sensitive to the steady-state pressure value but also is characterized by a strong rate-dependent component (i.e., a component affected by the time derivative of pressure signals). The existence of a rate-dependent component, and/or of a pure latency, may be influential during the first second after an acute cardiovascular perturbation, in response to pulsating pressure signals, or when analyzing the stability of the multi-

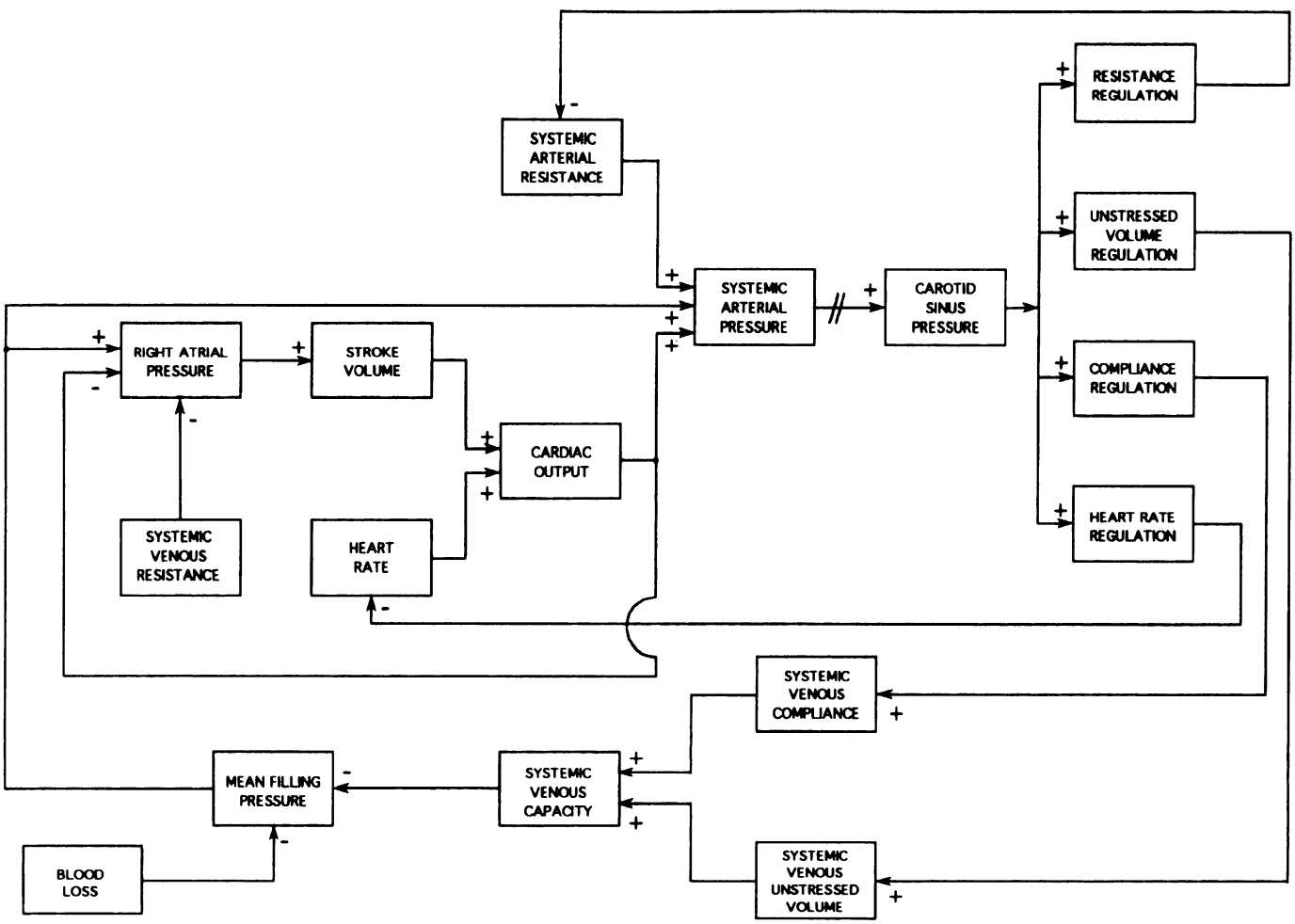

Fig. 4. Feedback regulatory mechanisms acting on the cardiovascular system according to the present model. R_{sv} has been maintained constant throughout the present simulations.

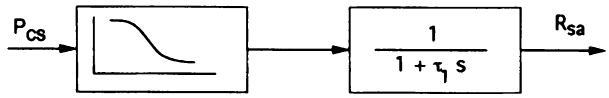

Fig. 5. Structure of the feedback mechanism working on R_{sa}. *Left*, mechanism static response, which exhibits a lower threshold and an upper saturation; *right*, mechanism dynamics, represented here as a simple 1st-order transfer function. τ_1, time constant of regulation. Mechanisms acting on heart rate and systemic venous V_u have been represented through an analogous schema.

feedback regulatory system [e.g., if one uses models to find out the genesis of vasomotor waves (28)]. Because in the present work attention is focused on stationary values rather than on transient phenomena, the possible role of rate-dependent components or of pure latencies in feedback loops has been neglected. These factors might easily be included in future works by modifying the second block of Fig. 5.

Finally, the feedback mechanism acting on systemic venous compliance has been simulated using a linear differential equation with a constant static gain instead of a sigmoidal characteristic. This choice has been adopted because the effect of the baroreflex mechanism on systemic venous compliance is quite modest (13, 31) and so does not permit identification of a sigmoidal nonlinear curve.

All of the parameters in the feedback regulatory mechanisms (i.e., the gains, upper and lower saturation levels, and time constants) have been assigned to reproduce the results of some experiments performed on animals in open-loop conditions. These are described in RESULTS. By contrast, the parameters of the controlled system have been directly taken from physiological literature. Because accurate assignment of these parameters is essential to attain correct simulations of cardiovascular dynamics, a brief critical analysis of the main data utilized is reported below. Finally, all model equations can be found in the APPENDIX.

ASSIGNMENT OF BASAL PARAMETERS FOR THE CONTROLLED SYSTEM

For a correct description of the baroreceptor response to carotid sinus stimulation, the basal parameters of the controlled system must be carefully assigned. These are cardiac frequency, resistances, compliances, and unstressed volumes of pulmonary and systemic compartments and, finally, the cardiac effectiveness of the heart (i.e., the slope and zero-intercept of the stroke volume-atrial pressure relationships) and cardiac capacities. In the physiological literature most of these parameters are usually expressed per unit tissue weight. This allows direct comparison to be made between clinical data obtained on human subjects and results derived through animal experiments.

As a general rule, we tried to use data taken from human subjects whenever possible, and we moved toward animal experiments only when accurate clinical results on humans were not available.

Resistances and Flow Values

A value for the four hydraulic resistances of Fig. 1, in basal conditions, has been computed starting from knowledge of the basal values of cardiac output and pressures in the cardiovascular system. Under resting conditions, cardiac output in humans is $\sim$75–80 $ml \cdot min^{-1} \cdot kg^{-1}$ (16, 25). We assumed a basal cardiac output in our model as high as 76.2 $ml \cdot min^{-1} \cdot kg^{-1}$ (i.e., 89 ml/s for a 70-kg man). The basal values of pressure (P) at the different points of the cardiovascular system (see Fig. 1) have been taken from data reported previously (1, 23). We assumed the following pressure values for the six compartments defined for *Eq. 1* (in mmHg): $P_{sa} = 100$, $P_{sv} = 5$, $P_{ra} = 4$, $P_{pa} = 17$, $P_{pv} = 7$, and $P_{la} = 6.5$. Finally, a value for the hydraulic resistances, in basal conditions, has been computed as the ratio of pressure drop to cardiac output.

Compliances

According to Safar and London (27) the total human compliance is $\sim$2.1 $ml \cdot mmHg^{-1} \cdot kg^{-1}$. Rothe (26) reports values of total compliance in the range of 2.0–2.3 $ml \cdot mmHg^{-1} \cdot kg^{-1}$ for humans and values of $\sim$2.5 $ml \cdot mmHg^{-1} \cdot kg^{-1}$ for dogs. In the present model we adopted the same value reported by Safar and London (27).

According to Rothe (25), $\sim$70% of this value may be ascribed to the systemic circulation, whereas the remaining 30% (0.63 $ml \cdot mmHg^{-1} \cdot kg^{-1}$) is provided by pulmonary vessels. By contrast, Safar and London (27) report a value for the total pulmonary compliance in humans as low as 0.45 $ml \cdot mmHg^{-1} \cdot kg^{-1}$, whereas an even lower value (0.3 $ml \cdot mmHg^{-1} \cdot kg^{-1}$) is reported by Shoukas (30) for the dog. In the present model we used the value reported by Safar and London (27) as the best compromise between different results. Therefore, we obtain a total systemic compliance equal to systemic arterial compliance + systemic venous compliance = 1.65 $ml \cdot mmHg^{-1} \cdot kg^{-1}$. It is worth noting that the value of total systemic compliance thus obtained lies in the range measured in most physiological experiments (13, 31, 32).

A distinction between systemic arterial and venous compliances may be reached by assuming (26) that the first parameter is $\sim$3% (0.049 $ml \cdot mmHg^{-1} \cdot kg^{-1}$) of the entire compliance of systemic vessels. A similar value is reported by Safar and London (27) for humans (0.044 $ml \cdot mmHg^{-1} \cdot kg^{-1}$). Values a little higher have been measured during animal experiments (31, 32). Because in the present work particular emphasis is placed on the experiments by Shoukas and Sagawa (32) on active control of systemic vascular capacity (see RESULTS), we decided to adopt the same percentage ratio of systemic arterial compliance to systemic venous compliance (C_{sa}/C_{sv}) reported in their work. We have $C_{sa}/C_{sv} \simeq 0.034$, and so $C_{sa} \simeq$ 0.056 $ml \cdot mmHg^{-1} \cdot kg^{-1}$.

Finally, we must distinguish in the model between pulmonary arterial and venous compliances. Unfortunately, just a few data can be found in the physiological literature on this point. Some authors (26, 30) claim that arterial pulmonary compliance is a significant portion of the total compliance of pulmonary vessels. We are aware of values obtained in animal experiments ranging between 0.05 and 0.12 $ml \cdot mmHg^{-1} \cdot kg^{-1}$ (11, 30). The value for arterial pulmonary compliance used in the present work (0.09 $ml \cdot mmHg^{-1} \cdot kg^{-1}$) lies in the central portion of the previous range and represents 20% of total pulmonary compliance.

Compliances of the right and left cardiac chambers (C_{ra} and C_{la}, respectively, in Fig. 1) were computed assuming that the average cardiac volume is $\sim$300 ml (see Table 1) and that unstressed volume is just one-sixth of the total cardiac volume (1).

Unstressed Volumes

Using the previous values of pressures and compliances, we can compute a basal value for the excess (or stressed) volume (V_e) in the vasculature. We have: $V_e = C_{sa} \cdot P_{sa} + C_{sv} \cdot P_{sv} + C_{pa} \cdot P_{pa} + C_{pv} \cdot P_{pv} \simeq 17.7$ ml/kg. This is just a little lower than the value reported by Rothe (25 ml/kg) (25).

To assign a value for the unstressed volumes in the four hematic compartments of Fig. 1, we considered typical distributions of blood volumes in pulmonary and systemic vessels, and in the cardiac chambers, as reported in the physiological

Table 1. *Percentage distribution of total blood volume in the 6 hematic compartments*

	Volume Distribution, %				
Ref. no.	12	1	21	21	present study
Subject	dog	human	dog	human	present model
V_{sa}	20.32	12.88	16.63	16.79	19.08
V_{sv}	64.36	64.17	66.57	69.99	65.21
V_{pa}	4.21	2.62	7.34	4.66	4.44
V_{pv}	3.71	11.31	4.50	3.52	5.61
V_{ra}	3.70	4.51	2.48	2.52	2.83
V_{la}	3.70	4.51	2.48	2.52	2.83

Blood volume (V) was measured in systemic arteries (sa), systemic veins (sv), pulmonary arteries (pa), pulmonary veins (pv), right heart (ra), and left heart (la).

literature (1, 12; Ref. 21, p. 45). Starting from these data, the percentage distribution shown in Table 1 can be computed: values used in the present model are shown in the last column. As is evident, all of these values agree fairly well with those reported in the physiological literature.

The values shown in Table 1 represent total blood volume in the corresponding compartment; that is, they comprise both unstressed and excess blood volume. Of course, the unstressed volume can easily be obtained as the difference between the total value shown in Table 1 and the corresponding excess volume computed as the product of pressure and compliance. To this end, a value of total blood volume as great as ~70 ml/kg has been used (25).

Cardiac Effectiveness

According to Rothe (25), the sensitivity of cardiac output to changes in right atrial pressure is ~35 $ml \cdot min^{-1} \cdot mmHg^{-1} \cdot kg^{-1}$. Other authors report experimental values in dogs and cats ranging between 25 and 48 $ml \cdot min^{-1} \cdot mmHg^{-1} \cdot kg^{-1}$ (see Refs. 13 and 25 for review). In the present model we adopted the same value as Rothe (25), which lies in the midportion of the physiological range. Starting from this value, the sensitivity of stroke volume-to-right atrial pressure changes (k_r in *Eqs. 11* and *13*) can be computed as the ratio of cardiac output sensitivity to heart frequency. When we assume a basal frequency (f) = 1.2 Hz, we obtain k_r = 0.486 $ml \cdot mmHg^{-1} \cdot kg^{-1}$.

According to several authors, the left heart is less sensitive than the right to filling pressure. Data reported in Rothe (25) indicate that the sensitivity of the left ventricle in dogs is about one-half that of the right ventricle. Greene and Shoukas (13) report experimental values ranging between 17 and 22 $ml \cdot min^{-1} \cdot mmHg^{-1} \cdot kg^{-1}$. We adopted a value of ~20.5 $ml \cdot min^{-1} \cdot mmHg^{-1} \cdot kg^{-1}$ for cardiac output sensitivity in the left heart. As a consequence, the sensitivity of stroke volume (k_l in *Eqs. 10* and *14*) becomes equal to 0.286 $ml \cdot mmHg^{-1} \cdot kg^{-1}$.

The last two parameters to be assigned are the intercepts of the stroke volume-atrial pressure relationships with the x-axis (i.e., $P_{la,0}$ and $P_{ra,0}$ in *Eqs. 10–14*). These parameters have been assigned by imposing that, when all hemodynamic quantities assume their basal value, the model settles at an equilibrium point.

All parameters of the controlled system are presented in Table 2. Notice that, to reproduce conditions occurring in a normal human, parameters per unit body weight have been multiplied by a standard weighing factor equal to 70 kg. However, this choice is not essential and has been adopted just to improve the clinical clearness of model simulation curves. Parameters per unit body weight may be maintained in the model equally well without altering the significance of the results obtained.

RESULTS

The model described above has been used to simulate the action of the carotid baroreflex in several conditions of physiological importance.

Initially, we have considered experiments performed in open-loop conditions, that is, conditions in which the carotid sinuses are isolated from the rest of the circulation and their transmural pressure is independently varied. Analysis of these experiments has been performed in two different stages. First, open-loop results have been employed to provide correct values for the parameters describing feedback regulatory actions. Subsequently, with all parameters given, the open-loop

Table 2. *Basal values of model parameters for the controlled cardiovascular system*

Volume, liters	
V_t	5.3
V_u	3.755
V_{sa}	1.011
$V_{u,sa}$	0.611
V_{sv}	3.455
$V_{u,sv}$	2.9
V_{pa}	0.235
$V_{u,pa}$	0.123
V_{pv}	0.297
$V_{u,pv}$	0.120
V_{la}	0.150
$V_{u,la}$	0.025
V_{ra}	0.150
$V_{u,ra}$	0.025
Resistance, $mmHg \cdot s \cdot ml^{-1}$	
R_{sa}	1.067
R_{sv}	0.0112
R_{pa}	0.112
R_{pv}	0.00562
Compliance, ml/mmHg	
C_{sa}	4
C_{sv}	111.111
C_{pa}	6.560
C_{pv}	25.37
C_{la}	19.23
C_{ra}	31.25
Pressure, mmHg	
P_{la}	6.5
P_{ra}	4
P_{sa}	100
P_{sv}	5
P_{pa}	17
P_{pv}	7
$P_{la,0}$	2.8
$P_{ra,0}$	1.82
Other model parameters	
Basal frequency (f)	1.2 Hz
Cardiac output	89 ml/s
LV stroke volume (S_l)	74.1 ml
RV stroke volume (S_r)	74.16 ml
LA cardiac effectiveness (k_l)	20.02 ml/mmHg
RA cardiac effectiveness (k_r)	34.02 ml/mmHg

All parameters per unit weight are multiplied by a weighing factor = 70 kg to simulate the hemodynamic of a normal human. V, volume [total (t) and unstressed (u)]; R, resistance; C, compliance; P, pressure; la,0 and ra,0 are x-intercepts of left and right heart, respectively; LV and RV, left and right ventricular, respectively; and LA and RA, left and right heart, respectively. Other subscripts are as in Table 1.

response of systemic arterial pressure and cardiac output has been simulated, as is seen from the interaction and superimposition of all feedback mechanisms involved.

Finally, the cardiovascular system dynamic has been considered in closed-loop conditions, assuming that the carotid sinuses are connected to the rest of the circulation, hence loaded by the systemic arterial pressure. Here we have simulated the hemodynamic response to an acute blood hemorrhage.

Open-Loop Experiments

Assignment of parameters for control mechanisms. To attain a quantitative understanding of the feedback mechanisms involved in carotid sinus stimulation, we have focused attention on two different groups of open-loop experiments.

In the first group of experiments (2, 6, 13, 19, 31), all hemodynamic quantities (including cardiac output and systemic venous pressure) were free to move from their initial basal level to a new value as a result of the imposed change in carotid sinus pressure. Of course, changes in heart rate and systemic resistance in these experiments are indicative of the strength of the corresponding mechanisms.

The second group of experiments was performed by Shoukas and Brunner (31) and Shoukas and Sagawa (32). These authors measured the baroreflex changes in systemic arterial pressure and in total vascular volume of vagotomized dogs, under conditions where cardiac output and systemic venous pressure were maintained constant artificially. Because of the constancy of cardiac output, changes in systemic arterial pressure in these experiments reflect only changes in systemic vascular resistance, whereas the amount of blood volume diverted from the cardiovascular system into an external reservoir allows changes in vascular capacity (compliance and unstressed volume) to be evaluated.

In their original experiments Shoukas and Sagawa (32) observed that the reflex effect on systemic compliance is negligible. Hence, they ascribed the entire alterations of vascular capacity to the unstressed volume active control. Later studies, however, revealed a small but evident increase of compliance ($\sim$22% according to Ref. 31; $\sim$10% according to Ref. 4) when raising carotid sinus pressure from 50 to 200 mmHg.

In the present work, we used data from Shoukas and Brunner (31) to assign the gain for the feedback mechanism working on venous compliance. After this value was assigned, the pattern of hemodynamic quantities vs. carotid sinus pressure in all of the aforementioned experiments was used to assign the sigmoidal characteristics for the mechanisms working on systemic arterial resistance, heart rate, and systemic venous unstressed volume. It is worth noting that, in most experiments, reflex changes in hemodynamic quantities are maximum in the central pressure range and rapidly decrease as soon as carotid sinus pressure approaches lower and higher saturation levels. This behavior further justifies the use of a sigmoidal characteristic for feedback regulatory mechanisms.

The simulation curves obtained by fitting model response to the aforementioned experimental data can be found in Figs. 6 and 7. Notice that all of these curves are expressed in terms of the percentage changes of quantities with respect to their basal value. This choice allows direct comparison between data characterized by different basal levels to be made.

The open-loop curve of systemic arterial resistance vs. carotid sinus pressure in Fig. 7*A* deserves a few comments. As pointed out by Borgdorff (3), peripheral beds are known to autoregulate within 10–15 s after a pressure change. This means that active changes in systemic resistance may reflect not only action of the baroreflex mechanism but also the simultaneous existence of blood flow autoregulation in vital organs like brain, kidney, or heart. Possible errors introduced by autoregulation on the systemic resistance response are noted in the DISCUSSION.

Figures 6 and 7 represent the static properties of the carotid baroreflex. To characterize its time dynamics, further data are needed. Shoukas and Sagawa (32) found that changes in capacity are completed within 3 min from beginning of the perturbation, with 60% of changes occurring within the first minute. Data reported by other authors, however (see Ref. 26 for more references), indicate that a complete reflex venoconstriction requires $\sim$1 min. It is possible that the longer time delay in the experiments by Shoukas and Sagawa (32) is imputable to the effect of the external reservoir, which artificially increases the time constant of the overall cardiovascular dynamics. For this reason, we preferred to use the values $\tau_3 = \tau_4 = 20$ s for the time constants of mechanisms acting on venous unstressed volume and venous compliance. The time constants of mechanisms controlling heart rate and systemic resistance have been taken from data reported previously (1, 7, 25). Notice that, according to those authors, heart rate regulation is the most rapid, being able to produce its effects within a few seconds from carotid sinus pressure alterations,

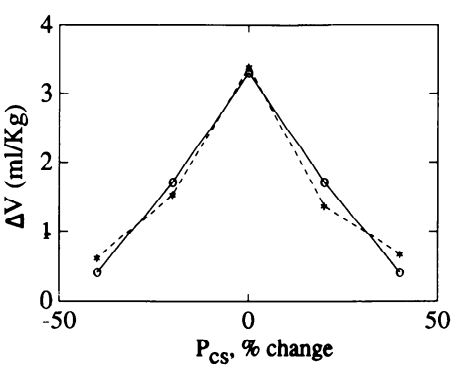

Fig. 6. Changes in total vascular volume (reservoir volume; ΔV) measured by Shoukas and Sagawa (32) in vagotomized dogs in response to a 18.5% change in P_{cs} (ΔP_{cs}/basal P_{cs} = 25 mmHg/135 mmHg $\simeq$ 18.5%) produced at different initial P_{cs} levels (*). Also shown are simulation results obtained with the present model in response to the same %change in P_{cs} and by giving proper values to parameters of the capacity control (○).

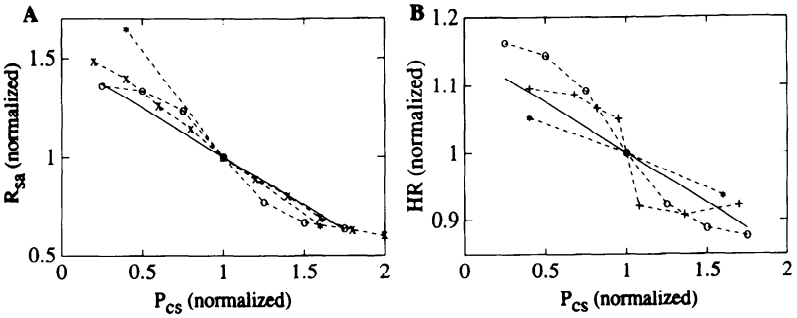

Fig. 7. %Changes in R_{sa} (*A*) and heart rate (HR; *B*) vs. %change in P_{cs}, simulated with the present model (○) and measured in experiments on vagotomized animals [solid line, regression line obtained by Maas-Moreno and Rothe (19) in the cat; other data are from Cox and Bagshaw (6) (×); Bolter and Ledsome (2) (+); Green and Shoukas (13) (*, HR) and Shoukas and Brunner (31) (*, R_{sa})]. These data were used to assign values for parameters in feedback regulatory mechanisms.

whereas the changes in systemic arterial resistance become complete only 10–20 s after the perturbation.

The numerical values of all parameters describing feedback regulatory actions are reported in Table 3.

Model validation. After all of the parameters were given, we used the model to simulate the pattern of systemic arterial pressure and cardiac output vs. carotid sinus pressure as measured in open-loop experiments (5, 6, 19, 29). Because these patterns are the result of complex interactions between all mechanisms described above, they can be used to validate the model and point out its possible values and limitations.

In Fig. 8, comparisons between model simulation curves and real data taken from vagotomized animals are presented. In particular, according to Fig. 8*A*, the pattern of systemic arterial pressure vs. carotid sinus pressure predicted by the model turns out in good agreement with most experimental data. This result supports the idea that the interaction between the four synergical mechanisms included in the model is sufficient to account quite well for the strength of the carotid sinus baroreflex without the need to assume further effectors for the regulation. Only in one case (6) does the experimental slope of systemic arterial pressure vs. carotid sinus pressure turn out significantly lower than that predicted by our model. The reason for this discrepancy can be understood by looking at the patterns of cardiac output vs. carotid sinus pressure shown in Fig. 8*B*.

As is clear from Fig. 8*B*, experimental data concerning cardiac output regulation exhibit a greater variance than those concerning systemic arterial pressure. In his review on baroreflex regulation, Sagawa (28) mentioned this phenomenon, imputing it to the great number of biophysical factors, some reflex, others mechanical, that simultaneously affect heart performance during carotid sinus activation. In particular, the results of our model are in good agreement with those obtained by Schmidt et al. (29) in vagotomized dogs, whereas data obtained by Maas-Moreno and Rothe (19) in the cat exhibit lower cardiac output regulation. Finally, data by Cox and Bagshaw (6) show adequate cardiac output control only in the central pressure range. This is why systemic arterial pressure regulation in the Cox and Bagshaw (6) experiments turns out significantly lower than in all other examined cases. Early autoregulation or differences in the strength of the capacity control may be responsible in part for the discrepancies in the cardiac output patterns evident in Fig. 8*B*.

To better understand the role of the venous capacity control, in Fig. 9, *A* and *B*, we present a comparison between simulation results obtained in open-loop conditions, first assuming that all of the feedback mechanisms shown in Fig. 4 are working together and subsequently assuming that only the mechanisms acting on heart rate and systemic resistance are functioning, whereas capacity control is impaired. As is clear from Fig. 9, the presence of a venous capacity control is of paramount importance to determine cardiac output and systemic arterial pressure changes during carotid sinus stimulation.

Table 3. *Model parameters for the feedback regulatory mechanisms*

r_1	17 mmHg
r_2	18.983 mmHg
r_3	11.546 mmHg
τ_1	6 s
τ_2	2 s
τ_3	20 s
τ_4	20 s
R_{max}	1.465 mmHg·s·ml^{-1}
R_{min}	0.67 mmHg·s·ml^{-1}
T_{max}	0.9545 s
T_{min}	0.712 s
V_{max}	3,267.5 ml
V_{min}	2,532.5 ml
G_4	0.15 ml/mmHg^2
$P_{cs,n}$	100 mmHg

r, Constant parameter; τ, time constant; R_{max} and R_{min}, upper and lower values of systemic resistance, respectively; T_{max} and T_{min}, upper and lower saturation values for the heart period; V_{max} and V_{min}, upper and lower saturation levels for $V_{u,sv}$; G_4, gain of regulation; and $P_{cs,n}$, carotid sinus pressure at hypothetical normal (basal) value.

Closed-Loop Experiments

Acute hemorrhage. Figure 10 shows the time pattern of the main hemodynamic quantities (systemic arterial pressure, cardiac output, systemic arterial resistance, and systemic venous pressure) simulated in closed-loop conditions in response to a 10% (i.e., 530 ml) acute blood loss. These curves were computed via three different simulations: in the first we assumed a passive cardiovascular system (i.e., no feedback mechanism operating); in the second we included only mechanisms acting on heart rate and systemic resistance; finally, in the last simulation we also introduced the presence of mechanisms

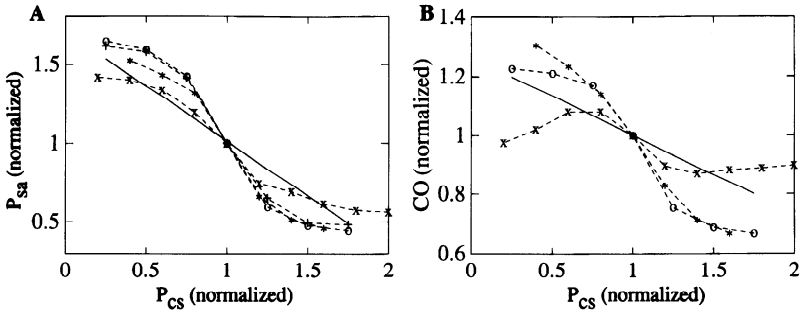

Fig. 8. %Changes in P_{sa} (*A*) and CO (*B*) vs. %change in P_{cs}, simulated with the present model (○) and measured in experiments on vagotomized animals [solid line, regression line obtained by Maas-Moreno and Rothe (19) in the cat; other data are from Schmidt et al. (29) (*); Cox and Bagshaw (6) (×); and Chen et al. (5) (+)]. Curves obtained are results of interaction among feedback mechanisms included in the model.

acting on systemic venous capacity (compliance and unstressed volume).

As is clear from Fig. 10, venous capacity control plays a pivotal role after acute hemorrhage, especially in maintaining filling pressure for the heart (Fig. 10*D*). If this mechanism were not present, cardiac output would decrease to very low levels (Fig. 10*B*) and the strength of mechanisms controlling heart rate and systemic arterial resistance would be inadequate to raise systemic arterial pressure toward physiological levels. By contrast, as is evident in Fig. 10*A*, the existence of a significant capacity control permits restoration of more adequate systemic arterial pressure, at the same time avoiding excessive reflex changes in heart rate and systemic arterial resistance (Fig. 10*C*).

Finally, to further validate the model, we compared the simulated steady-state values of hemodynamic quantities after 10% hemorrhage with analogous data measured in an experiment on the dog (17). In the present experiment, percentage changes of the main hemodynamic quantities after hemorrhage were measured at various stages of denervation, including vagal denervation (absence of the aortic sinus reflex) and carotid sinus plus vagal denervation (i.e., absence of all baroreflex mechanisms). The results, shown in Fig. 11, demonstrate that model predictions agree with the experimental data fairly well, in the case of both vagal (Fig. 11*A*) and total (Fig. 11*B*) denervation.

Role of nonlinear compliances. One of the main simplifications introduced in the present model was the use of linear pressure-volume relationships. As pointed out by Drees and Rothe (10), whereas the use of linear compliances is probably acceptable in the physiological pressure range, extrapolation of the observed results to the case of highest blood volume changes may produce unacceptable errors.

To test the entity of errors introduced by the use of linear compliances and the range of validity of the present model, we found it useful to simulate various hemorrhages of increasing severity using either linear or nonlinear (exponential) pressure-volume curves for the vascular compartments. Nonlinear pressure-volume characteristics were obtained by imposing the same basal values of pressure, volume, and compliance as in the linear case (see Fig. 12) and by assuming that the vessels collapse at small negative transmural pressure values. The baroreflex control of unstressed volume was simulated, in the nonlinear case, by horizontally shifting the entire pressure-volume curve, whereas, for the sake of simplicity, the mild control of compliance was neglected. Mathematical details on the nonlinear characteristics employed can be found in the APPENDIX.

Figure 13 shows a comparison between the values of systemic arterial pressure (Fig. 13*A*) and cardiac output (Fig. 13*B*) obtained with the model at 100 s from acute hemorrhages using either linear or nonlinear characteristics for vascular compartments. As is evident from Fig. 13, the use of linear pressure-volume characteristics does not cause significant error as long as blood volume changes do not exceed ~15% of normal. When more severe hemorrhages are simulated, the effect of nonlinearitites in pressure-volume curves becomes important to prevent the cardiovascular system from an excessive arterial pressure fall.

DISCUSSION

The main purpose of the present work was to investigate the functional importance of the baroreflex venous capacity control in accurate quantitative terms. To this end, we used mathematical modeling and computer simulations. The importance of this approach for studying complex physiological systems in general and cardiovascular regulation in particular (1, 15, 16) has been underlined by several authors in the past three decades.

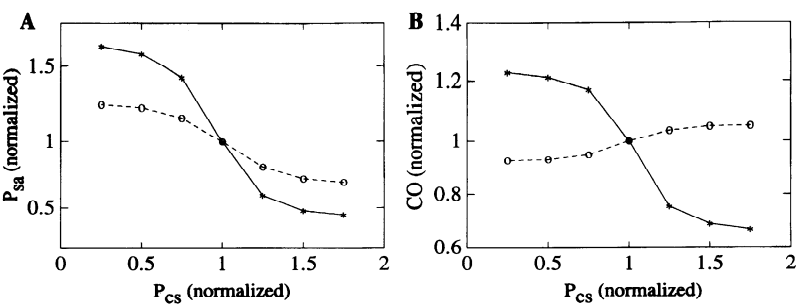

Fig. 9. Comparison between %changes in P_{sa} (*A*) and CO (*B*) vs. %change in P_{cs} simulated with the present model when all feedback mechanisms are working properly (solid line) and when mechanisms acting on systemic venous capacity are impaired (dotted line). The pivotal role played by venous capacity control in CO regulation is evident.

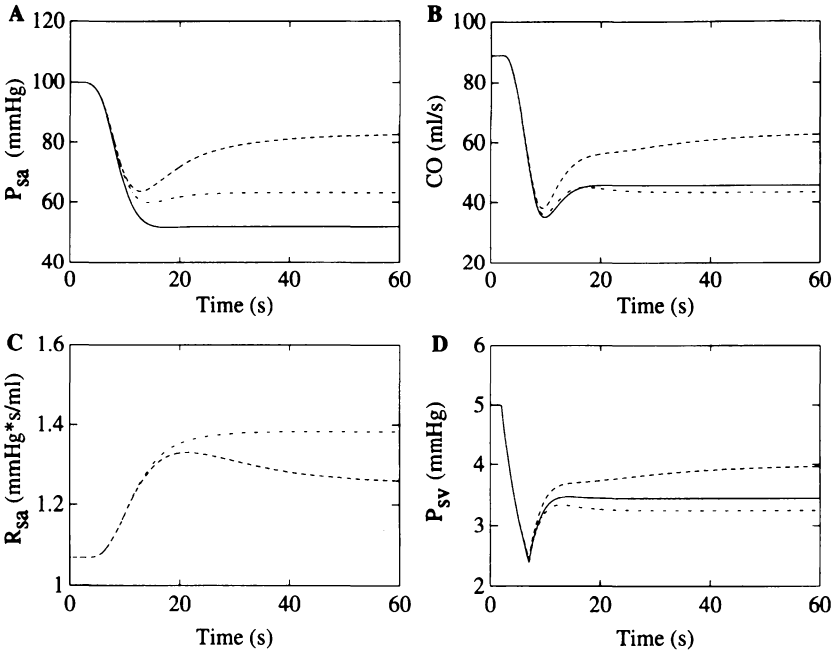

Fig. 10. Time pattern of P_{sa}, CO, R_{sa}, and P_{sv} simulated with the model in response to an acute 10% (i.e., 530 ml) hemorrhage. ——, Curves obtained assuming that the entire carotid baroreflex is impaired (passive cardiovascular system); –·–·, curves obtained including only mechanisms working on HR and R_{sa} (capacity control impaired); – – –, curves obtained with all feedback mechanisms functioning. Also in these simulations, the significant role of the baroreflex capacity control is evident.

First, as pointed out above, strong nonlinearities in the cardiovascular system and in regulatory actions preclude application of the superimposition of the effects. This means that the reciprocal importance of the various mechanisms involved in the regulation, and the final result of their complex relationships, is usually different from the sum of the individual actions separately investigated. As a consequence, a purely qualitative approach to the problem, based for instance on a verbose description of the main phenomena involved, may often fail to grasp some fundamental aspects of system behavior and may lead to inconsistent or misleading conclusions.

Second, we can note that the great amount of experimental data gathered in recent years on short-term cardiovascular homeostasis often risks being underutilized, or insufficiently understood, if they are not inserted into a more general theoretical framework. Mathematical models may favor this synthesis process, at the same time providing a new tool for comparing data coming from different experiments and analyzing the reasons for contradictory results.

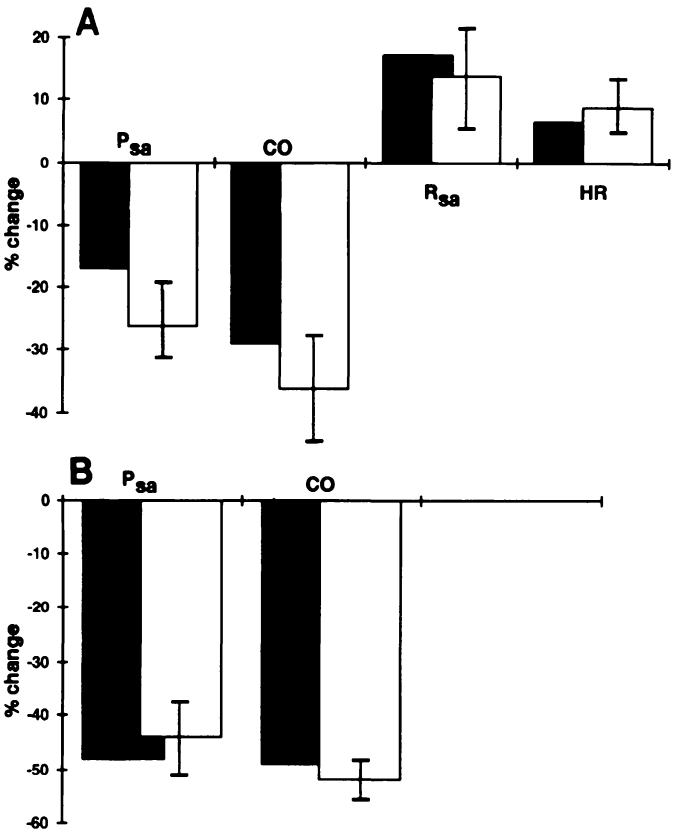

Fig. 11. Comparison among steady-state values of P_{sa}, CO, R_{sa}, and HR %changes, simulated with the present model in response to a 10% acute hemorrhage and measured by Hosomi and Sagawa (17) in the dog at 1.5 min from an hemorrhage of the same severity. Solid bars, theoretical values; open bars, experimental values. *A*: vagal denervation (absence of sinoaortic reflex). *B*: carotid sinus + vagal denervation (complete absence of the baroreflex control). Bars are SD.

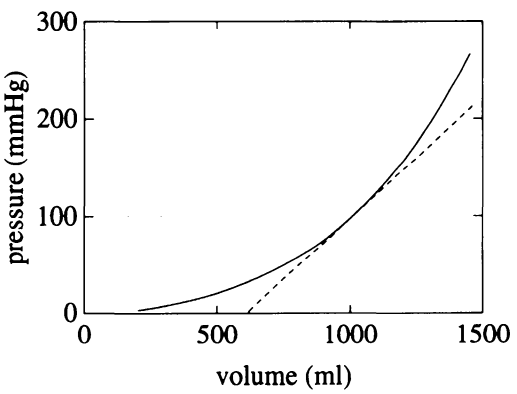

Fig. 12. Nonlinear pressure-volume characteristic of systemic veins (solid line) used to simulate deep hemorrhages. This characteristic was obtained by imposing passage for the same basal point, with the same basal value of compliance as in the linear case (dotted line), and by assuming that the vessel collapses at small negative transmural pressure values (−2 mmHg). Similar nonlinear characteristics were used for other vascular compartments.

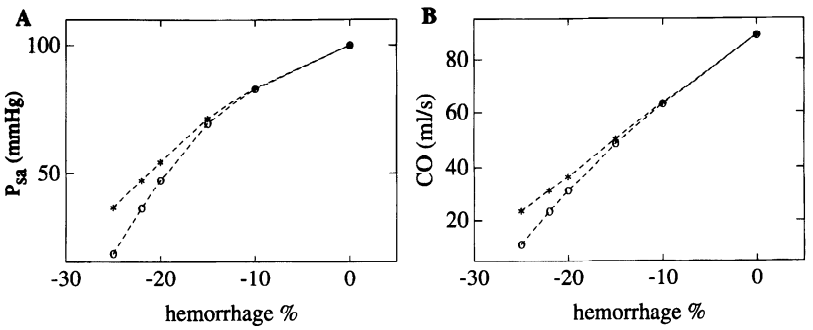

Fig. 13. Effect of different hemorrhages (10–25% of total blood volume) on P_{sa} and CO, simulated with the model using either linear (○) or nonlinear (*) pressure-volume curves for vascular compartments. When blood volume changes exceed ~15% of total blood volume, use of linear pressure-volume curves may lead to significant errors.

The model presented in the present study synthesizes several factors able to affect short-term cardiovascular regulation. At present, model attention is focused merely on the carotid baroreflex, for which enough experimental data taken from animal experiments are available.

The main conclusion that one can draw from the present simulation results is that active constriction of capacitive veins is of great importance in short-term compensation for small losses of blood or fluid, permitting rapid homeostasis to be attained without excessive reflex changes in cardiac performance (i.e., heart rate and contractility) and in peripheral hemodynamics (systemic arterial resistance). In fact, according to the present model (Fig. 10*A*) 10% of blood volume removal from the cardiovascular system in the absence of reflex venous compensation causes systemic arterial pressure to fall down to ~60% of normal. The same perturbation, however, provokes no more than a 20% decrease in systemic arterial pressure within 1 min when capacity is actively controlled by the baroreflex regulatory system. In particular, capacity changes seem to constitute a powerful method for restoring filling pressure for the heart. It is worth noting that this mechanism may be of the greatest value not only after blood hemorrhage but also during pooling of blood into the extremities or fluid extravasation from the circulation to the tissue. Although the same idea was first formulated by Shoukas and Sagawa (32) and further supported by Drees and Rothe (10) and Shoukas and Brunner (31), an accurate quantitative analysis of the problem was still not available.

As is evident from Figs. 9 and 11, reproduction of experimental results cannot be warranted by mechanisms acting only on heart rate and on systemic arterial resistance. In particular, if the capacity control is impaired, model cardiac output decreases with lowering carotid sinus pressure in open-loop experiments (Fig. 9*B*). This is due to both a decrease in central venous pressure (preload), consequent on blood volume shifting from veins to arteries, and a simultaneous increase in systemic arterial pressure (afterload). However, as is evident in Fig. 8*B*, various experimental results agree in showing that cardiac output does not decrease but rather increases significantly during carotid sinus hypotension, although wide quantitative differences can be found among individual data. The model is able to explain this experimental behavior imputing it partly to the reflex increase in heart rate and, above all, to active reduction of systemic venous capacity.

It is worth noting that our open-loop simulation results agree quite well with the experimental data by Schmidt et al. (29). By contrast, data by Maas-Moreno and Rothe (19) exhibit a lower gain for cardiac output regulation. This result might confirm the observation by others (synthesized in Ref. 25), according to whom capacity control in the cat might be less pronounced than in the dog. Finally, results by Cox and Bagshaw (6) differ from the others in that cardiac output exhibits sufficient regulation only in a limited pressure range. As soon as carotid sinus pressure reaches a value ~25% higher or lower than normal, cardiac output shows a direct dependence on carotid sinus pressure. According to the present model (Fig. 9*B*), this behavior seems to be characteristic of conditions with exhausted capacity control. In confirmation of this hypothesis, it is interesting to observe that the results by Cox and Bagshaw (6) may be reproduced quite well with the present model (unpublished simulations) simply by assuming a smaller regulatory range for the mechanism acting on venous unstressed volume. In other words, according to the present theoretical framework, animals in the experiments by Cox and Bagshaw (6) seem to have insufficient capacity regulation reserve.

The latter consideration raises the problem of how much the strength of the capacity control may vary among individuals and whether the values used in our simulations really belong to a physiological range. In the present work (Fig. 5), data have been taken from the well-known experiments by Shoukas and Sagawa (32) on vagotomized dogs. In those experiments, changing carotid sinus pressure from 75 to 200 mmHg caused an overall 7.5 ml/kg change in reservoir volume with a maximum sensitivity (~0.14 ml/kg per mmHg) at 135 mmHg. Previous studies, performed in less accurate conditions, provided results that seem consistent with those by Shoukas and Sagawa (24; see Ref. 32 for more references). Subsequently, however, Muller-Ruchholtz et al. (22) reported a much lower sensitivity for the capacity control (with a maximum sensitivity of only 0.07 ml/kg per mmHg). Finally, a more recent study by Shoukas and Brunner (31) gave values for the capacity control significantly higher than those shown in Fig. 5. The total change in the reservoir volume induced by carotid sinus pressure alterations was as high as 12.35 ml/kg. These differences in the sensitivity of mechanisms acting on venous capacity may, at least in part, account for the profound variability in the pattern of cardiac output observed during carotid sinus activation.

It is now important to critically examine some limits of this model as well as objections that might be moved against the main conclusions of the present work.

A first possible cause of error may arise from the presence of peripheral blood flow autoregulation. Although several authors state that the effect of autoregulation on systemic arterial resistance becomes evident with a time constant of at least 5–10 min (16), the presence of an early autoregulation (time constant of ~10–15 s) also has been observed by some authors (e.g., Ref. 3). Early autoregulation is probably imputable to those organs (like the heart, the kidney and, especially, the brain) able to respond within a few seconds to local perfusion pressure changes.

Because of the presence of early autoregulation, changes in systemic arterial resistance shown in Fig. 7*A* might not only be imputable to action of the carotid baroreflex, but also reflect local vascular adjustments at the level of peripheral organs. From Figs. 7 and 8, we can say that, during the open-loop experiments, autoregulation may act in synergism with the baroreflex mechanism, since both cardiac output and systemic arterial pressure as well as systemic resistance change in the same direction. This means that the baroreflex open-loop gain might be overestimated looking at the results of Figs. 7 and 8. By contrast, during hemorrhage experiments, autoregulation may act in antagonism with the baroreflex control, thus causing a decrease in systemic arterial resistance and systemic arterial pressure. This might contribute to explaining some of the differences between model and experimental results evident in Fig. 11. Better understanding of the relationship between baroreflex control and autoregulation might be achieved in future works by presenting a separate description of organs with distinct regulatory response (i.e., organs with prompt autoregulation, like brain, heart, kidney, etc., and organs which especially participate to baroreflex adjustments, like the splanchnic circulation).

As to the possible effect of nonlinearities in vascular compliances, the results of Fig. 13 indicate that the use of linear pressure-volume curves is acceptable as long as moderate blood volume changes (~10 or 15% of total) are simulated. The use of exponential pressure-volume curves (Fig. 12) extends the range of model applicability to lower and higher pressures; however, it also may exhibit some disadvantages with respect to the use of linear relationships. In particular, whereas exponential pressure-volume curves are probably correct at very low values of pressure and volume, when vascular smooth muscle is almost completely relaxed, they might be inappropriate in the range where smooth muscle responds with active contraction. Active changes in compliance, induced by the baroreflex mechanism, can be simulated rather easily using linear pressure-volume curves (see Fig. 2), whereas this requires more unwieldy computations when nonlinear curves are adopted.

Another relevant point is that adjustments in cardiac output may be achieved not only by means of active venous capacity changes but also by a combined reflex increase in heart rate and cardiac contractility. One might speculate that the central role of the capacity venous control in our model is merely a consequence of having underestimated the importance of the other two cardiac mechanisms.

Indeed, in our model the stroke volume-atrial pressure relationship has been assumed to be independent of carotid sinus pressure. As described in QUALITATIVE MODEL DESCRIPTION, *Feedback Regulating Actions* this assumption is equal considering that the increase in cardiac contractility caused by baroreflex activation almost exactly compensates for the decrease in stroke volume induced by tachycardia. This choice was based on data reviewed in Downing (8) and Downing and Gardner (9) and, in part, on the results of Greene and Shoukas (13) and Kostiuk et al. (18).

Downing and Gardner (9) report experimental patterns of stroke volume vs. atrial pressure measured in the feline at different carotid sinus pressure levels. From their curves it is evident that, when afterload is maintained constant, carotid sinus pressure exerts only a negligible influence on the stroke volume-atrial pressure curve.

Data by Greene and Shoukas (13) are a little more controversial. However, when the afterload was kept constant, the authors observed that "...the variation in stroke volume with carotid sinus pressure was not consistent in every dog.... In six of the dogs, the curve for carotid sinus pressure = 50 was above that for carotid sinus pressure = 200. In four of the dogs the opposite was true".

Further results by Kostiuk et al. (18) indicate a 38% increase in the slope of the cardiac output-atrial pressure curve by changing carotid sinus pressure from 150 to 75 mmHg in vagotomized animals with a constant afterload. However, it is difficult to assess what portion of this change is imputable to the reflex increase in heart frequency and what portion actually reflects an increase in slope of the stroke volume relationship. In our model, a profound decrease in carotid sinus pressure causes a 25% rise in heart frequency (Fig. 7*B*). This result can explain about two-thirds of the changes in the cardiac function curve reported by Kostiuk et al. (18).

The previous results, taken together, lead us to conclude that, in vagotomized animals, the stroke volume-atrial pressure relationship is either unaffected, or just mildly affected, by the carotid baroreflex control.

Another important point to be recognized is that the strength of the mechanism acting on the heart rate is difficult to determine experimentally in vagotomized conditions, since cutting the vagus often alters the basal level of heart frequency. Of course, comparison of percentage change in heart rate performed starting from different baselines may be questionable, even though such comparison is necessary to perform model validation.

Based on these premises, it is not at all surprising that large differences in percentage change in heart rate and cardiac function curves are sometimes observed during carotid sinus pressure changes. The values used in this work have been taken in acceptable agreement with some experimental curves (Figs. 8*B* and 11) and should

be considered a reasonable reproduction of a typical physiological subject.

Another important point is that the simulation results of Figs. 10, 11, and 13 are intended to be significant only in the very first phase after acute blood losses (no more than 2 min). As pointed out by Drees and Rothe (10), in fact, passive transcapillary fluid shift and viscoelastic creep become a primary source of pressure compensation after ~1–2 min.

Finally, we want to focus attention on a possible limitation of our model, that is, the supposed constancy of systemic venous resistance. Especially during severe hemorrhage, it is possible that venous resistance increases significantly due to a reduction in intravascular pressure. This mechanism, in turn, may cause a further dramatic decrease in cardiac output through a reduction in atrial pressure. Quantification of this phenomenon is difficult and requires more sophisticated modeling of the dynamics of collapsible veins.

The present model was intended to represent just a first step toward more accurate quantitative analysis of short-term cardiovascular homeostasis. Inclusion of the aortic arch baroreflex, description of venous collapsibility, analysis of stability margins in the presence of pure latencies, and investigation of pulsatile rather than stationary regimens may be the subjects of future studies.

APPENDIX: QUANTITATIVE MODEL DESCRIPTION

The Cardiovascular System

Equations describing cardiovascular system dynamics can be written starting from the electric analog of Fig. 1. We shall use the subscripts sa, sv, pa, and pv to represent a quantity or a parameter that belongs to the systemic arterial, systemic venous, pulmonary arterial, or pulmonary venous compartment, respectively, and subscripts ra and la for the left and right heart, respectively. By denoting cardiac output from the left and right ventricles as $\dot{q}_l$ and $\dot{q}_r$ and applying the mass preservation principle, the following basic state equations can be written, where C is compliance, P is pressure, R is resistance, and t is time.

Mass preservation at systemic arteries

$$C_{sa} = \frac{dP_{sa}}{dt} = \dot{q}_l - \frac{P_{sa} - P_{sv}}{R_{sa}} \tag{2}$$

Mass preservation at pulmonary arteries

$$C_{pa} = \frac{dP_{pa}}{dt} = \dot{q}_r - \frac{P_{pa} - P_{pv}}{R_{pa}} \tag{3}$$

Mass preservation at pulmonary veins

$$C_{pv} = \frac{dP_{pv}}{dt} = \frac{P_{pa} - P_{pv}}{R_{pa}} - \frac{P_{pv} - P_{la}}{R_{pv}} \tag{4}$$

Mass preservation at left heart

$$C_{la} \frac{dP_{la}}{dt} = \frac{P_{pv} - P_{la}}{R_{pv}} - \dot{q}_l \tag{5}$$

Mass preservation at right heart

$$C_{ra} \frac{dP_{ra}}{dt} = \frac{P_{sv} - P_{ra}}{R_{sv}} - \dot{q}_r \tag{6}$$

Finally, the mass preservation principle in the systemic veins can be warranted without adding a further state variable to the model. In fact, it is sufficient to impose preservation of the total blood volume contained in the overall cardiovascular system. We thus can write

$$C_{sv} \cdot P_{sv} = V_t + V_i - V_u - (C_{sa} \cdot P_{sa} + C_{pa} \cdot P_{pa} + C_{pv} \cdot P_{pv} + C_{ra} \cdot P_{ra} + C_{la} \cdot P_{la}) \tag{7}$$

where V_t is a constant parameter representing the total blood volume initially contained in the cardiovascular system, the additional variable V_i is an input quantity representing the amount of blood volume injected into or subtracted from the cardiovascular system during the simulation, and the term in parentheses represents the excess blood volume contained in the remaining five compartments. Of course, we have unstressed volume (V_u)

$$V_u = V_{u,sa} + V_{u,pa} + V_{u,sv} + V_{u,pv} + V_{u,ra} + V_{u,la} \tag{8}$$

By denoting with the injection rate into the systemic venous compartment (i_{sv}; see Fig. 1), we have

$$V_i(t) = \int_0^t i_{sv}(\tau) d\tau \tag{9}$$

where τ is a temporal variable. As is seen in RESULTS, this input is essential to simulate the carotid baroreflex response to acute blood volume perturbations.

To solve the system of *Eqs. 2–9*, $\dot{q}_l$ and $\dot{q}_r$ must be specified. According to the well-known Frank-Starling mechanism, stroke volume increases monotonically with atrial pressure in the physiological pressure range. We thus can write

$$S_l = k_l \cdot (P_{la} - P_{la,0}) \tag{10}$$

$$S_r = k_r \cdot (P_{ra} - P_{ra,0}) \tag{11}$$

where S_l and S_r are stroke volume from the left and right ventricles, respectively; P_{la} and P_{ra} are left and right atrial pressures, respectively; k_l and k_r are cardiac effectiveness of left and right ventricles, respectively; and $P_{la,0}$ and $P_{ra,0}$ are constant parameters denoting the intercept of the cardiac output-atrial pressure relationship with the x-axis, respectively.

An important question to be recognized is that the relationships in *Eqs. 10* and *11* may be influenced by several physiological factors, especially heart frequency and sympathetic changes in contractile force. An increase in heart frequency alone would cause this relationship to be shifted down, due to a decrease in the interval allowed for cardiac filling. By contrast, an increase in contractility may cause this curve to be shifted up. Because both of the effects are known to occur during baroreflex activation, we can write, for the left heart

$$k_l = k_{l,0} \cdot \frac{\gamma(P_{cs})}{\phi[f(P_{cs})]} \tag{12}$$

where $k_{l,0}$ is a constant parameter; γ and ϕ are two positive monotonic functions describing the effect on the slope of the stroke volume-atrial pressure curve of a baroreflex increase in cardiac contractility and in heart frequency, respectively; and f is heart frequency; in the present work, both changes are

assumed to be mediated by alterations in carotid sinus pressure (P_{cs}).

As discussed in QUALITATIVE MODEL DESCRIPTION, *Feedback Regulatory Actions*, we lack clear evidence about variations in the slope of the stroke volume-atrial pressure curve during carotid baroreflex activation. Moreover, according to some authors (20), the increase in cardiac force induced by sympathetic stimulation parallels the increase in heart frequency. Hence, we assumed that the ratio $\gamma(P_{cs})/\phi[f(P_{cs})]$, and thus parameter k_l in *Eq. 10*, remains constant throughout the present simulations. A similar assumption was adopted as to the right heart as well (i.e., as to parameter k_r in *Eq. 11*). However, it is worth noting that these assumptions may be justified only with reference to carotid baroreflex activation or sympathetic stimulation experiments, when both cardiac force and heart rate may change in similar ways. In different conditions, such as atrial pacing or vagal stimulation, the ratio γ/ϕ and the slope of the stroke volume curve might vary significantly.

Of course, cardiac output, in both the left and right hearts, can be computed as the product of frequency and stroke volume. As is well known, however, cardiac performance is also significantly affected by the load against which the heart is working. To describe this phenomenon, the previous expressions for stroke volume should be multiplied by a corrective factor, which takes the afterload into account. In particular, we assumed that, whenever the arterial pressure increases above normal, cardiac work increases with the square root of downstream pressure. Because cardiac work is the product of pressure and stroke volume, the previous assumption also implies that stroke volume is inversely proportional to the square root of arterial pressure. We thus can express cardiac output as follows

$$\dot{q}_r = k_r \cdot f \cdot (P_{ra} - P_{ra,0}) \cdot L_r$$

$$\begin{cases} \text{if} \quad P_{pa} > P_{pa,n} \quad \text{then} \quad L_r = \sqrt{P_{pa,n}/P_{pa}} \\ \text{if} \quad P_{pa} < P_{pa,n} \quad \text{then} \quad L_r = 1 \end{cases} \tag{13}$$

$$\dot{q}_l = k_l \cdot f \cdot (P_{la} - P_{la,0}) \cdot L_l$$

$$\begin{cases} \text{if} \quad P_{sa} > P_{sa,n} \quad \text{then} \quad L_l = \sqrt{P_{sa,n}/P_{sa}} \\ \text{if} \quad P_{sa} < P_{sa,n} \quad \text{then} \quad L_l = 1 \end{cases} \tag{14}$$

where subscript n denotes a quantity at its hypothetical normal (basal) value and L_r and L_l are effect of afterload on right and left cardiac output, respectively.

Equations 2–9 and *13–14* allow the pattern of the main hemodynamic quantities (P_{sv}, P_{pv}, P_{sa}, P_{pa}, P_{ra}, P_{la}, $\dot{q}_r$, and $\dot{q}_l$) to be computed as a function of the hemodynamic parameters of the model, that is, heart frequency (f), cardiac effectiveness (k_l and k_r), hydraulic resistances and compliances (R_{sa}, R_{sv}, R_{pa}, R_{pv}, C_{sa}, C_{sv}, C_{pa}, C_{pv}, C_{ra}, and C_{la}), unstressed volumes ($V_{u,sa}$, $V_{u,sv}$, $V_{u,pa}$, $V_{u,pv}$, $V_{u,ra}$, and $V_{u,la}$), and total initial blood volume (V_t). The input for the model is the amount of fluid injected into or subtracted from the cardiovascular system at the level of systemic veins (i_{sv}; see *Eq. 9*).

These equations describe the controlled system or plant, that is, the cardiovascular system in the absence of regulatory actions. During carotid sinus stimulation, however, a few parameters are known to be affected by the baroreflex response. Mathematical equations describing these feedback actions, as to both their strength and time pattern, are described below.

Feedback Regulatory Actions

Feedback regulatory actions are assumed to work on the cardiovascular system in response to carotid sinus stimulation according to the general block diagram of Fig. 5. Hence, the following equations for feedback regulatory actions can be written.

Control of systemic arterial resistance

$$dR_{sa}/dt = (-R_{sa} + \sigma_R)/\tau_1$$

$$\sigma_R = \frac{R_{max} + R_{min} \cdot \exp[(P_{cs} - P_{cs,n})/r_1]}{1 + \exp[(P_{cs} - P_{cs,n})/r_1]} \qquad \text{with} \quad R_{max} > R_{min} \tag{15}$$

where P_{cs} is the transmural pressure at the carotid sinus level, τ_1 is the time constant of the regulatory action, the sigmoidal function $\sigma_R(P_{cs})$ describes the nonlinear static gain, R_{max} and R_{min} represent the upper and lower saturation values of systemic resistance, and r_1 is a constant parameter related to the central slope of the sigmoidal curve. According to *Eq. 15*, the baroreflex mechanism causes a rise in systemic resistance in response to a decrease in carotid sinus pressure.

It is to be noted that, in *Eq. 15*, we used a value for carotid sinus transmural pressure distinct from that for systemic arterial pressure. This choice was adopted to simulate open-loop experiments, that is, experiments in which carotid sinuses are isolated from the rest of the circulation and their transmural pressure is independently varied. Hence, in open-loop conditions, the two quantities P_{cs} and P_{sa} are distinct. By contrast, in closed-loop conditions, when the carotid sinuses are loaded by the systemic arterial pressure, we have $P_{sa} = P_{cs}$.

Control of heart period

$$dT/dt = (-T + \sigma_T)/\tau_2$$

$$\sigma_T = \frac{T_{max} + T_{min} \cdot \exp[(P_{cs,n} - P_{cs})/r_2]}{1 + \exp[(P_{cs,n} - P_{cs})/r_2]} \qquad \text{with} \quad T_{max} > T_{min} \tag{16}$$

where $T = 1/f$ denotes the heart period; σ_T is nonlinear static gain of the mechanism; T_{max} and T_{min} are upper and lower saturation values for the heart period, respectively; and r_2 is a constant parameter. According to *Eq. 16*, lowering carotid sinus pressure causes a decrease in the heart period, and hence an increase in heart frequency, in an effort to restore a normal pressure level through a rise in cardiac output.

Control of systemic venous unstressed volume

$$dV_{u,sv}/dt = (-V_{u,sv} + \sigma_V)/\tau_3$$

$$\sigma_V = \frac{V_{max} + V_{min} \cdot \exp[(P_{cs,n} - P_{cs})/r_3]}{1 + \exp[(P_{cs,n} - P_{cs})/r_3]} \qquad \text{with} \quad V_{max} > V_{min} \tag{17}$$

where σ_V is the sigmoidal static curve and V_{max} and V_{min} are upper and lower saturation levels for $V_{u,sv}$, respectively. According to *Eq. 17*, a reduction of carotid sinus pressure causes a decrease in the unstressed volume of systemic veins. The latter may contribute to restore a more appropriate pressure level both via a redistribution of the available blood between arteries and veins and by increasing the filling pressure for the heart.

Control of systemic venous compliance. As specified in RESULTS, the mild alterations in venous compliance reported in

the literature in response to carotid sinus stimulation do not permit identification of a sigmoidal shape for the regulation gain analogous to that shown in Fig. 5 and employed in *Eqs. 15–17*. Hence, we preferred to assume a linear steady-state relationship between pressure and compliance. This corresponds to the following differential equation

$$dC_{sv}/dt = [-(C_{sv} - C_{sv,n}) + G_4 \cdot (P_{cs} - P_{cs,n})]/\tau_4 \quad (18)$$

where G_4 and τ_4 are the gain and time constant of regulation, respectively. According to *Eq. 18*, lowering carotid sinus pressure causes a moderate linear decrease in systemic venous compliance.

The system of *Eqs. 15–18* describes the main regulatory actions that, according to the present model, act on the cardiovascular system after carotid sinus stimulation. Joined with *Eqs. 2–9* and *13–14*, these allow the overall cardiovascular response to be simulated in several experimental conditions of physiological and clinical importance. In particular, experiments have been divided into two different classes: those performed in open-loop conditions ($P_{cs} \neq P_{sa}$) and those performed with the carotid sinus directly connected to the rest of the circulation ($P_{cs} = P_{sa}$). Moreover, when simulating the open-loop experiments by Shoukas and Sagawa (32) (see Fig. 6 in RESULTS), cardiac output from the left and right ventricles and systemic venous pressure have been maintained at their normal level throughout the simulations. Hence, *Eqs. 13–14* have been replaced with the simpler equations, $\dot{q}_l = \dot{q}_r = 89$ ml/s, and *Eq. 7* with $P_{sv} = 5$ mmHg. In this condition, of course, total blood volume is not constant. The changes of vascular volume in the model correspond to the amount of blood volume exchanged with an external reservoir in the experiments by Shoukas and Sagawa (32).

Finally, integration of differential equations has been performed on 386–486 IBM compatible personal computers, using the fourth-order Runge-Kutta method with adjustable step length.

Nonlinear Pressure-Volume Characteristics

As specified in QUALITATIVE MODEL DESCRIPTION, *The Controlled System*, we found it useful to repeat some simulations using nonlinear pressure-volume curves for the vascular compartments. The equations employed have the following form

$$P_j = P_{j,0} \cdot \{\exp [k_j \cdot (V_j - V_{j,0})^{1.5}/V_j] - 1\} \quad \text{with} \quad j = \text{sa, sv, pa, pv} \quad (19)$$

where subscript j indicates the compartment. The exponent 1.5 in *Eq. 19* has been chosen because the pressure-volume curve of relaxed vessels often exhibits a more rapid rise than that predicted by a simple monoexponential characteristic. The parameter $P_{j,0}$ has been taken equal to 2 mmHg for all compartments. Because, according to *Eq. 19*, $-P_{j,0}$ represents the value at which compliance becomes infinite, the previous choice is similar in supposing that vessels collapse at small negative transmural pressure levels. Values for the parameters k_j and $V_{j,0}$ have been given by constraining the pressure-volume curve to pass through the basal point ($V_{j,n}$, $P_{j,n}$), with the same basal value of compliance, $C_{j,n} = (dV_j/dP_j)_n$, as in the linear case (see Table 2 and Fig. 12). The presence of an unstressed volume control in the systemic veins has been simulated by shifting *Eq. 19* to the right or to the left of the same amount as that predicted by *Eq. 17*, whereas, for the sake of simplicity, the effect of a compliance control was neglected.

Address for reprint requests: M. Ursino, Dipartimento di Elettronica, Informatica e Sistemistica, Università degli studi di Bologna, Viale Risorgimento 2, I-40136 Bologna, Italy.

Received 28 July 1993; accepted in final form 7 June 1994.

REFERENCES

1. **Beneken, J. E. W., and B. De Wit.** A physical approach to hemodynamic aspects of the human cardiovascular system. In: *Physical Bases of Circulatory Transport: Regulation and Exchange*, edited by E. B. Reeve and A. C. Guyton. Philadelphia, PA: Saunders, 1967, p. 1–45.
2. **Bolter, C. P., and J. R. Ledsome.** Effect of cervical sympathetic nerve stimulation on canine carotid sinus reflex. *Am. J. Physiol.* 230: 1026–1030, 1976.
3. **Borgdorff, P.** Peripheral resistance after cardiac output reduction in the barodenervated cat. *Circ. Res.* 52: 7–15, 1983.
4. **Brunner, M. J., A. A. Shoukas, and C. L. MacAnespie.** The effect of the carotid sinus baroreceptor reflex on blood flow and volume redistribution in the total systemic vascular bed. *Circ. Res.* 48: 274–285, 1981.
5. **Chen, H. I., C. Y. Chai, C. S. Tung, and H. C. Chen.** Modulation of the carotid baroreflex function during volume expansion. *Am. J. Physiol.* 237 (*Heart Circ. Physiol.* 6): H153–H158, 1979.
6. **Cox, R. H., and R. J. Bagshaw.** Baroreceptor reflex control of arterial hemodynamics in the dog. *Circ. Res.* 37: 772–786, 1975.
7. **Donald, D. E., and A. J. Edis.** Comparison of aortic and carotid baroreflexes in the dog. *J. Physiol. Lond.* 215: 521–538, 1971.
8. **Downing, S. E.** Baroreceptor regulation of the heart. In: *Handbook of Physiology. The Cardiovascular System. The Heart.* Bethesda, MD: Am. Physiol. Soc., 1979, sect. 2, vol. I, chapt. 17, p. 621–652.
9. **Downing, S. E., and T. H. Gardner.** Reflex regulation of ventricular work performance. *Yale J. Biol. Med.* 39: 73–89, 1966.
10. **Drees, J. A., and C. F. Rothe.** Reflex venoconstriction and capacity vessel pressure-volume relationship in dogs. *Circ. Res.* 34: 360–373, 1974.
11. **Engelberg, J., and A. B. DuBois.** Mechanics of pulmonary circulation in isolated rabbit lungs. *Am. J. Physiol.* 196: 401–414, 1959.
12. **Green, H. D.** Circulatory system: physical principles. In: *Medical Physics*, edited by O. Glasser. Chicago, IL: Year Book, 1950, vol. II, p. 228–251.
13. **Greene, A. S., and A. A. Shoukas.** Changes in canine cardiac function and venous return curves by the carotid baroreflex. *Am. J. Physiol.* 251 (*Heart Circ. Physiol.* 20): H288–H296, 1986.
14. **Grodins, F. S.** Integrative cardiovascular physiology: a mathematical synthesis of cardiac and blood vessel hemodynamics. *Q. Rev. Biol.* 34: 93–116, 1959.
15. **Guyton, A. C., T. G. Coleman, and H. J. Granger.** Circulation: overall regulation. *Annu. Rev. Physiol.* 34: 13–46, 1972.
16. **Guyton, A. C., C. E. Jones, and T. G. Coleman.** *Circulatory Physiology: Cardiac Output and Its Regulation.* Philadelphia, PA: Saunders, 1973.
17. **Hosomi, H., and K. Sagawa.** Effect of pentobarbital anesthesia on hypotension after 10% hemorrhage in the dog. *Am. J. Physiol.* 236 (*Heart Circ. Physiol.* 5): H607–H612, 1979.
18. **Kostiuk, D. P., K. Sagawa, and A. A. Shoukas.** Modification of the flow-generating capability of the canine heart-lung compartment by the carotid sinus baroreceptor reflex. *Circ. Res.* 38: 546–553, 1976.
19. **Maas-Moreno, R., and C. F. Rothe.** Carotid baroreceptor control of liver and spleen volume in cats. *Am. J. Physiol.* 260 (*Heart Circ. Physiol.* 29): H254–H259, 1991.
20. **Manning, J. W., and P. Lindgren.** Inhibition of sympathetic tone and the effects of cardiac contractile force by baroreceptor reflex. In: *Baroreceptors and Hypertension*, edited by P. Kezdi. Oxford, UK: Pergamon, 1967, p. 201–210.
21. **Milnor, W. R.** *Hemodynamics.* Baltimore, MD: William & Wilkins, 1982, p. 45.
22. **Muller-Ruchholtz, E. R., E. Grund, F. Hauer, and E. R. Lapp.** Effect of carotid pressoreceptor stimulation on integrated systemic venous bed. *Basic Res. Cardiol.* 74: 467–476, 1979.

23. **Parmley, W. W., and L. Talbot.** Heart as a pump. In: *Handbook of Physiology. The Cardiovascular System. The Heart.* Bethesda, MD: Am. Physiol. Soc., 1979, sect. 2, vol. I, chapt. 11, p. 429–460.
24. **Rashkind, W. J., D. H. Lewis, J. B. Henderson, D. F. Heiman, and R. B. Dietrick.** Venous return as affected by cardiac output and total peripheral resistance. *Am. J. Physiol.* 175: 415–423, 1953.
25. **Rothe, C. F.** Reflex control of veins and vascular capacitance. *Physiol. Rev.* 63: 1281–1342, 1983.
26. **Rothe, C. F.** Venous system: physiology of the capacitance vessels. In: *Handbook of Physiology. The Cardiovascular System. Circulation.* Bethesda, MD: Am. Physiol. Soc., 1983, sect. 2, vol. III, pt. 1, chapt. 13, p. 397–452.
27. **Safar, M. E., and G. M. London.** Venous system in essential hypertension. *Clin. Sci.* 69: 497–504, 1985.
28. **Sagawa, K.** Baroreflex control of systemic arterial pressure and vascular bed. In: *Handbook of Physiology. The Cardiovascular System. Circulation.* Bethesda, MD: Am. Physiol. Soc., 1983, sect. 2, vol. III, pt. 2, chapt. 14, p. 453–496.
29. **Schmidt, R. M., M. Kumada, and K. Sagawa.** Cardiac output and total peripheral resistance in carotid sinus reflex. *Am. J. Physiol.* 221: 480–487, 1971.
30. **Shoukas, A. A.** Pressure-flow and pressure-volume relations in the entire pulmonary vascular bed of the dog determined by two-port analysis. *Circ. Res.* 37: 809–818, 1975.
31. **Shoukas, A. A., and M. Brunner.** Epinephrine and the carotid sinus baroreceptor reflex. Influence on capacitive and resistive properties of the total systemic vascular bed of the dog. *Circ. Res.* 47: 249–257, 1980.
32. **Shoukas, A. A., and K. Sagawa.** Control of total systemic vascular capacity by the carotid sinus baroreceptor reflex. *Circ. Res.* 33: 22–32, 1973.